Crystallization Kinetics of Poly(L-Lactide)/Carbonated Hydroxyapatite Nanocomposite Microspheres

Wen You Zhou,[1] Bin Duan,[2] Min Wang,[2] Wai Lam Cheung[2]

[1]*Discipline of Orthodontics, Faculty of Dentistry, The University of Hong Kong, Hong Kong*
[2]*Department of Mechanical Engineering, The University of Hong Kong, Hong Kong*

Received 31 January 2009; accepted 5 April 2009
DOI 10.1002/app.30527
Published online 27 May 2009 in Wiley InterScience (www.interscience.wiley.com).

ABSTRACT: Microspheres consisting of carbonated hydroxyapatite (CHAp) nanoparticles and poly(L-lactide) (PLLA) have been fabricated for use in the construction of osetoconductive bone tissue engineering scaffolds by selective laser sintering (SLS). In SLS, PLLA polymer melts and crystallizes. It is therefore necessary to study the crystallization kinetics of PLLA/CHAp nanocomposites. The effects of 10 wt% CHAp nanoparticles on the isothermal and nonisothermal crystallization behavior of PLLA matrix were studied, using neat PLLA for comparisons. The Avrami equation was successfully applied for the analysis of isothermal crystallization kinetics. Using the Lauritzen-Hoffman theory, the transition temperature from crystallization Regime II to Regime III was found to be around 120°C for both neat PLLA and PLLA/CHAp nanocomposite. The combined Avrami-Ozawa equation was used to analyze the nonisothermal crystallization process, and it was found that the Ozawa exponent was equal to the Avrami exponent for neat PLLA and PLLA/CHAp nanocomposite, respectively. The effective activation energy as a function of the relative crystallinity and temperature for neat PLLA and PLLA/CHAp nanocomposite under the nonisothermal crystallization condition was obtained by using the Friedman differential isoconversion method. The Lauritzen-Hoffman parameters were also determined from the nonisothermal crystallization data by using the Vyazovkin-Sbirrazzuoli equation. CHAp nanoparticles in the composite acted as an efficient nucleating agent, enhancing the nucleation rate but at the same time reducing the spherulite growth rate. This investigation has provided significant insights into the crystallization behavior of PLLA/CHAp nanocomposites, and the results obtained are very useful for making good quality PLLA/CHAp scaffolds through SLS. © 2009 Wiley Periodicals, Inc. J Appl Polym Sci 113: 4100–4115, 2009

Key words: biomaterials; carbonated hydroxyapatite; crystallization; nanocomposites; poly(L-lactide)

INTRODUCTION

Medical-profession-accepted and the US Food and Drug Administration-approved biodegradable polymers have been used for tissue engineering applications over the last 2 decades because of their good biocompatibility and acceptable biodegradation properties. Poly(L-lactide) (PLLA) is a linear aliphatic biodegradable polymer and has been widely studied for use as a scaffolding material for human body tissue regeneration.[1–3] The enzymatic and nonenzymatic hydrolysis rate of PLLA strongly depends on its chemical properties (such as molecular weight and weight distribution) and physical properties (such as crystallinity and morphology). Crystallinity plays an important role in the degradation behavior of biodegradable polymers. It is well known that the crystallinity and morphology of semicrystalline polymers such as PLLA are greatly influenced by their thermal history. Therefore, the crystallization kinetics of PLLA should be carefully studied and correlated to its processing method as it forms a basis for the interpretation of the scaffold properties. The isothermal bulk crystallization kinetics of PLLA has been studied by a number of research groups, covering a temperature range from 70 to 165°C.[4–7] But only a few studies were conducted on the nonisothermal crystallization kinetics of neat PLLA. Miyata and Masuko[6] reported that PLLA could not crystallize and remained amorphous when the cooling rate was higher than 10°C/min. The knowledge on nonisothermal crystallization kinetics is useful for modeling real industrial processes such as cast film extrusion, which generally takes place at a nonconstant cooling rate.[8]

Particulate bioceramic reinforced polymer composites can combine the strength and stiffness of bioactive inorganic fillers with the flexibility and toughness of biodegradable organic matrices. Carbonated hydroxyapatite (CHAp) is a promising

Correspondence to: W. Y. Zhou (wyzhou@hku.hk).
Contract grant sponsor: Hong Kong Research Grants Council (GRF research grant); contract grant number: HKU 7118/05E.
Contract grant sponsor: University of Hong Kong.

bioactive material for bone substitution as it is bioresorbable and also more bioactive *in vivo* than stoichiometric hydroxyapatite. PLLA/CHAp nanocomposite has been developed and used for constructing bone tissue engineering scaffolds through SLS.[9,10] In the SLS process, the laser beam selectively fuses powdered material by scanning crosssections generated from a 3D digital description of the part (e.g., from a CAD file or scan data) on the surface of a powder bed. After each crosssection is scanned, the powder bed is lowered by one layer thickness, a new layer of material is applied on top, and the process is repeated until the part is completed. Sintering is a thermal fusion process for bonding particles into solid structures.[11] The physical process of SLS may involve multiple cycles of melting (full or partial) and crystallization of polymer to produce solid parts. In a separate development, Ignjatovic et al.[12] used hot pressing to produce PLLA/hydroxyapatite (HAp) biocomposite for medical applications. They found that the crystallinity of PLLA decreased after the process time of hot pressing was increased. However, the crystallization kinetics of PLLA/HAp composite was not fully evaluated. Currently, little is known about the effects of nanosized HAp or CHAp on PLLA crystallization behavior under isothermal or nonisothermal conditions. To better understand the *in vitro* behavior of the PLLA/CHAp nanocomposite scaffolds produced by SLS, it is necessary to study the crystallization kinetics of the nanocomposite and the neat PLLA. In the current investigation, the overall crystallization kinetics and spherulitic morphologies of neat PLLA and PLLA/CHAp nanocomposite were studied by means of differential scanning calorimetry (DSC) and polarized optical microscopy (POM). In the isothermal crystallization study, the sample was rapidly cooled from the melt and allowed to crystallize at a prefixed temperature. In the nonisothermal crystallization study, the sample was allowed to crystallize upon cooling at various rates from the melt to room temperature.

EXPERIMENTAL

Materials

The PLLA used was Medisorb® 100L 1A (Lakeshore Biomaterials, AL) with an inherent viscosity of 1.9 dL/g. It was supplied in the pellet form: 1 mm in diameter and 3 mm in length. The M_n and M_w of this polymer were determined to be 1.23×10^5 and 2.21×10^5, respectively, by gel permeation chromatography using *N*-methyl pyrrolidone as the solvent. The CHAp nanospheres were synthesized in-house using a nanoemulsion method without surfactants.[13] The mean particle size of the resultant CHAp nanoparticles was about 20 nm. Poly(vinyl alcohol) (PVA, Sigma-Aldrich, cold water soluble) was used as the emulsifier and dichloromethane (DCM, A.R.) used as the organic solvent to dissolve PLLA for microsphere fabrication.

Fabrication of PLLA Microspheres

PLLA microspheres were fabricated using a conventional oil-in-water (O/W) emulsion/solvent evaporation technique.[14] The resultant PLLA microspheres were washed and lyophilized to obtain dry powders.

Fabrication of PLLA/CHAp nanocomposite microspheres

PLLA/CHAp nanocomposite microspheres were produced using a solid-in-oil-in-water (S/O/W) emulsion/solvent evaporation method as reported previously.[14] Briefly, the CHAp nanoparticles were dispersed in the PLLA-dichloromethane solution by ultrasonification and homogenization to form an S/O nanosuspension. The nanosuspension was mixed with PVA solution to fabricate PLLA/CHAp nanocomposite microspheres. PLLA/CHAp microspheres containing 10 wt % of CHAp nanoparticles were used in this investigation.

Thermal property measurement and crystallization study

The thermal properties of PLLA and PLLA/CHAp nanocomposites and their crystallization behavior were studied using a Perkin Elmer Pyris 6 differential scanning calorimeter (DSC, MA) and with the heating and cooling rates of 10°C/min. The apparatus was calibrated with pure indium and zinc standards at various scanning rates. Dry nitrogen gas at a flow rate of 20 mL/min was used to purge through the DSC cell during all measurements. A new sample was used for each measurement to eliminate the effect of thermal degradation. Each test was repeated three times to ensure accuracy. The effect of previous heat treatments (thermal history) can significantly affect the shape of the DSC curve for semicrystalline polymers. To compare the thermal data of PLLA with values found in the literature, a standardized thermal history is desirable and can be achieved by a heat-cool-reheat DSC method.[15] In this method, the first heating process destroys any previous thermal history (assuming the maximum temperature is sufficient to remove any remaining nuclei without causing sample degradation), the cooling process imposes a known thermal history on the sample, and the second heating process allows the sample to be measured with a known thermal history. In this investigation, the samples were

heated from room temperature to 200°C with a heating rate of 10°C/min (Step 1) and held there for 5 min to eliminate the thermal history (Step 2, annealing). Then samples were quenched to room temperature at cooling rate of 40°C/min (Step 3) and reheated to 200°C to probe the melting point (Step 4). The glass transition temperature (T_g) was determined before annealing; whereas the cold crystallization and melting temperature (T_{cc} and T_m, respectively) and the enthalpy of cold crystallization and fusion (ΔH_{cc} and ΔH_m, respectively) were determined after annealing. The crystallinity (X_c) of the PLLA matrix was calculated from the reheating DSC data using the following equation[16,17]:

$$X_c\ (\%) = \frac{\Delta H_m - \Delta H_{cc}}{X_{PLLA}\Delta H_m^0} \times 100 \quad (1)$$

where ΔH_m is the measured enthalpy of fusion, ΔH_{cc} is the cold crystallization enthalpy of PLLA during the heating process, X_{PLLA} is the PLLA weight percentage in the composite. ΔH_m^0 is the enthalpy change of 100% crystalline PLLA, which is 135 J/g, as was estimated by Miyata and Masuko[6] from the linear relationship between exothermic enthalpy change with density.

Isothermal crystallization

To investigate the overall kinetics of isothermal melt crystallization, PLLA samples (weighing between 10 and 15 mg) were heated in the DSC from 30 to 200°C at a rate of 80°C/min and held at 200°C for 5 min to allow through melting. They were then cooled at 50°C/min to the predetermined crystallization temperatures (T_c) and allowed to crystallize. The high cooling rate of 50°C/min was used to minimize crystallization of PLLA during cooling.[7] The heat evolved during crystallization was recorded as a function of time.

Polarized optical microscopy

The spherulitic morphologies of neat PLLA and PLLA/CHAp nanocomposites were observed using a polarized optical microscope (POM, Metallux II, Leitz, Germany) equipped with a hot stage (Leitz 350, Germany) and a temperature controller (Partlow, MIC 8200, USA). Samples weighing about 5 mg were sandwiched between two microscope cover slides and melted at 200°C to form thin films. The samples were held at the same temperature for 5 min to destroy any thermal history and then cooled to isothermal crystallization temperatures of 110, 120, and 130°C. The temperature of the hot stage was kept constant within 0.1°C and optical photographs were taken using a digital color camera (Samsung, SCC-101 BP, China).

Nonisothermal crystallization

For nonisothermal melt crystallization, the samples were quickly heated from 30 to 200°C at a heating rate of 80°C/min and maintained at 200°C for 5 min in the DSC cell to destroy any nuclei that might act as seed crystals. The samples were then cooled to 30°C at constant rates of 0.5, 1.0, 2.5, 5.0, 7.5, and 10°C/min, respectively. The exothermic crystallization peaks were recorded as a function of temperature.

RESULTS AND DISCUSSION

Thermal properties

The thermal properties of neat PLLA and PLLA/CHAp were needed for the crystallization kinetics analysis and therefore determined through DSC. Typical DSC curves of neat PLLA and PLLA/CHAp nanocomposites were shown in Figure 1(a,b), and thermal characteristics were listed in Table I. It can be seen that the addition of CHAp nanoparticles decreased the glass transition temperature (T_g) and cold crystallization temperature (T_{cc}) of PLLA and slightly increased its melting temperature (T_m). These results suggest that the CHAp nanoparticles promoted initial glass transition and cold crystallization of the PLLA matrix, indicating an enhanced crystallization ability of PLLA in the presence of CHAp, which might behave as nucleating agents. Similar observations were made recently in the PLLA/nano-clay system[18] with a decrease of T_g value of 1-2°C. The addition of 10 wt % CHAp nanospheres reduces the T_g of PLLA by about 2.89°C. It has been suggested that nanosheet particles are much favorable for the improvement of thermal stability compared to more isotropic geometry fillers, such as nanospheres.[19] However, the detailed mechanisms for the decreased T_g value of PLLA after addition of CHAp are not clear. ΔH_{cc} and ΔH_m represent the cold crystallization enthalpy and enthalpy of fusion, respectively, from which the absolute degrees of crystallinity, X_c, of melt-quenched PLLA and PLLA/CHAp can be calculated using eq. (1). In theory, the lowest possible value for X_c is 0, which is for totally amorphous polymers. The negative value for the neat PLLA is most likely a result of the accuracy level of the DSC experiment. A more realistic interpretation is that $X_c \approx 0$, i.e., the melt-quenched PLLA was more or less amorphous. In fact, our result has confirmed Miyata and Masuko's result[6] that PLLA could not crystallize and remained amorphous when cooled at rates higher

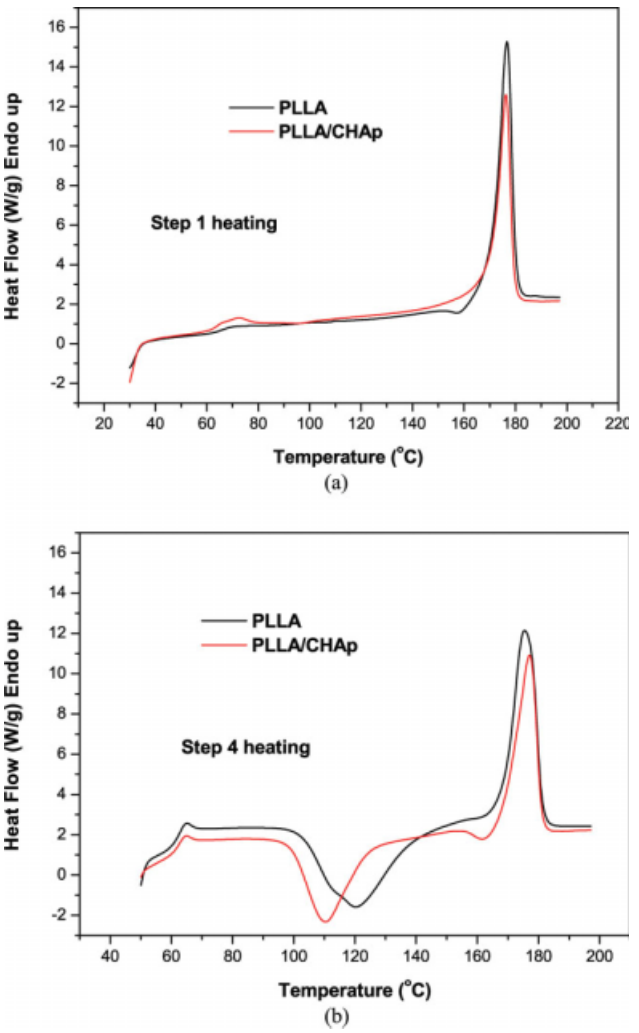

Figure 1 DSC curves for the neat PLLA and PLLA/CHAp nanocomposites: (a) heating before annealing (Step 1) and (b) heating after annealing (Step 4). [Color figure can be viewed in the online issue, which is available at www.interscience.wiley.com.]

than 10°C/min. In the current investigation, the samples were quenched at the rate of 50°C/min. In comparison, the PLLA/CHAp nanocomposite gave a small but nonnegligible X_c value of 4%. One possible explanation is that the CHAp nanoparticles acted as a nucleating agent and promoted limited amount of crystallization even under such rapid cooling condition. During the DSC tests, cold crystallization occurred, giving rise to ΔH_{cc}. The value of ΔH_{cc} for PLLA/CHAp is slightly lower than that of the neat PLLA. This is probably because some crystallizable material had been consumed during the cooling process and the amount left for the cold crystallization process had dropped. Finally, the slightly higher ΔH_m value of the nanocomposite, compared with neat PLLA, indicates that the CHAp nanoparticles enhanced the overall crystallinity of the PLLA matrix.

Isothermal crystallization kinetics

The isothermal crystallization kinetics of neat PLLA and PLLA/CHAp nanocomposite was studied by cooling the melt rapidly (50°C/min) to the crystallization temperature, ranging from 90 to 140°C. The exothermal curves were then recorded as a function of crystallization time, and the results are shown in Figure 2. The values of crystallization enthalpy (ΔH_c) were obtained from the exothermal curves and are listed in Table II. Clearly, ΔH_c increased with increasing crystallization temperature for both neat PLLA and PLLA/CHAp. At low isothermal crystallization temperatures, the addition of CHAp seemed to have little influence on the crystallization enthalpy of the PLLA matrix. At higher isothermal crystallization temperatures, however, it decreased the crystallization enthalpy significantly compared with that of neat PLLA. Such change may imply a drop in the amount of crystals formed or a lower degree of perfection of the crystals or both. The presence of a large amount of nanosized CHAp particles (10 wt%) was likely to increase the melt viscosity, thus making it more difficult for the macromolecular chains to pack into perfect crystals.

The kinetics of isothermal crystallization can be described by the well-known Avrami Equation.[8] A time-dependent relative volumetric crystallinity X_t for an isothermal crystallization process can be expressed as:

$$X_t = 1 - \exp(-kt^n) \tag{2}$$

or

$$\log[-\ln(1 - X_t)] = \log k + n \log t \tag{3}$$

where t is the time, n is the Avrami exponent, and k is the overall crystallization rate constant, which contains contributions from both nucleation and growth. Parameters n and k can be obtained from the slope and intercept, respectively, of the Avrami

TABLE I
Thermal Properties of Melt-Quenched Neat PLLA and PLLA/CHAp Nanocomposite

Samples	T_g (°C)	T_{cc} (°C)	ΔH_{cc} (J/g)	T_m (°C)	ΔH_m (J/g)	X_c (%)
PLLA	66.74 ± 0.15	120.13 ± 0.11	37.98 ± 2.75	175.22 ± 0.24	36.79 ± 0.43	−0.9
PLLA/CHAp	63.85 ± 0.30	110.31 ± 0.10	34.27[a] ± 2.91	177.1 ± 0.33	39.59[a] ± 1.93	4.0

[a] Values of ΔH_{cc} and ΔH_m for PLLA/CHAp have been normalized to unit mass of the PLLA matrix.

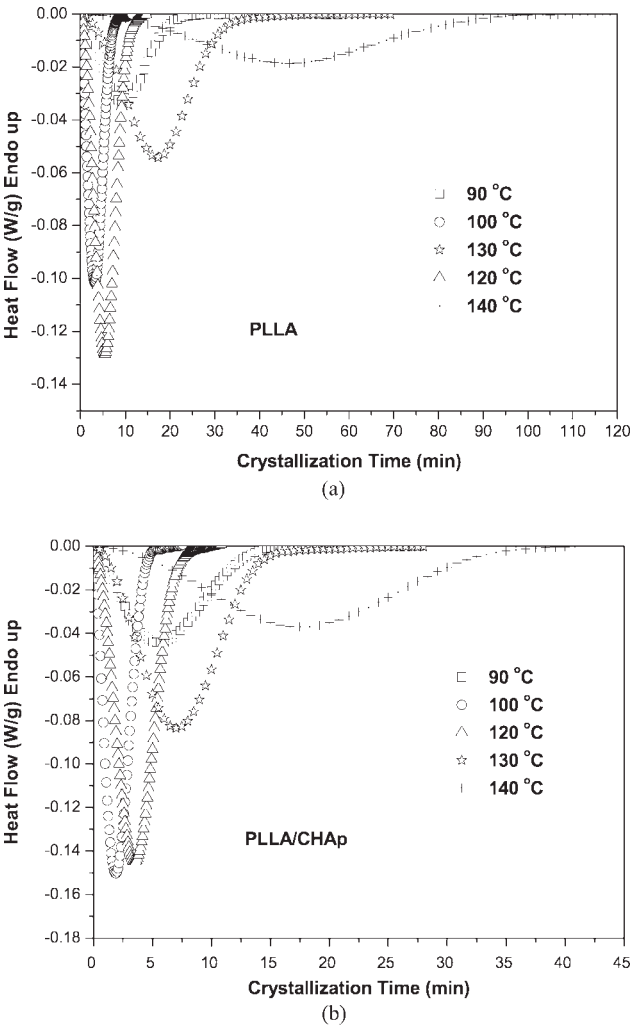

Figure 2 DSC thermograms obtained from isothermal crystallization of (a) neat PLLA and (b) PLLA/CHAp nanocomposite (The crystallization temperatures are indicated in the graphs).

plot of log $[-\ln(1 - X_t)]$ versus log t. According to Lorenzo et al.[20] the relative volumetric crystallinity (X_t) can be calculated as:

$$X_t = \frac{W_c}{W_c + (\rho_c/\rho_a)(1 - W_c)} \tag{4}$$

where ρ_c and ρ_a are the fully crystalline and fully amorphous polymer densities, respectively. For commonly existed α form of PLLA, $\rho_c = 1.283$ g/cm^3 and $\rho_a = 1.248$ g/cm^3.[21] The determination of the absolute crystallinity is not needed for the analysis of the crystallization kinetics, and the degree of relative mass crystallinity, W_c, can be calculated as:

$$W_c = \frac{\Delta H_t}{\Delta H_{total}} = \frac{\int_0^t (dH/dt)dt}{\int_0^\infty (dH/dt)dt} \tag{5}$$

taking ΔH_t as the enthalpy variation as function of the time spent at a given crystallization temperature, whereas ΔH_{total} is the maximum enthalpy value reached at the end of the isothermal crystallization process. Both quantities can be obtained from the isothermal curve by integration.

Figure 3 displays the typical Avrami double-logarithmic plots for neat PLLA and PLLA/CHAp. The Avrami parameters n and k were obtained from the plots and are listed in Table II. Figure 4 shows the corresponding curves of relative degree of crystallinity with time (symbols) for neat PLLA and PLLA/CHAp obtained from the experimental crystallization isotherms as exhibited in Figure 2. In a recent investigation,[20] it was suggested that the choice of relative crystallinity range was very important for a good Avrami fit. The initial data points ($X_t < 3\%$) may not be accurate due to experimental errors during the primary crystallization stage and hence do not need to be under serious consideration. The secondary crystallization process produces nonlinearity in the Avrami plot so the relative crystallinity range should be chosen during the primary crystallization process. According to their study,[20] a relative crystallinity range of 3–20% is sufficient for a good Avrami fit. To check the validity of the Avrami method for studying the isothermal crystallization kinetics of neat PLLA and PLLA/CHAp, the variations of the relative crystallinity (X_t) for the respective isothermal crystallization temperatures were calculated using the values of n and k listed in Table II, and the results are shown as solid lines in Figure 4. The calculated results fit very well with the experimental data, indicating that the Avrami method can be used to study the isothermal crystallization process in the current investigation in case some of the common problems were avoided.[20] It can be seen from Table II that the coefficient of determination of the Avrami plot, r^2, is near unity, which also suggests a good fit between the theoretical and experimental results in the relative crystallinity range of 3–20% as recommended by Lorenzo et al.[20] The valid values of n and k are essential to the Lauritzen-Hoffman (LH) analysis by using $t_{0.5}$ data.

The Avrami exponent (n) is composed of two terms:

$$n = n_d + n_n \tag{6}$$

where n_d represents the dimensionality of the growing crystals and this quantity can only have, as values, the integer numbers 1, 2, or 3, corresponding to one-, two- or three-dimensional entities that are formed. In the case of polymers, only 2 and 3 are commonly obtained as they represent axialites (two-dimensional lamellar aggregates) and spherulites (three-dimensional aggregates of radial lamellae), respectively. The time dependence of the nucleation is represented by n_n. In principle, its value should

TABLE II
Properties and Parameters Obtained from the Isothermal Crystallization of Neat PLLA and PLLA/CHAp Nanocomposite

Samples	T_c (°C)	ΔH_c (J/g)	ΔH_c^* (J/g)	n	k (min^{-n})	r^2	$t_{0.5}^*$ (min)	$t_{0.5}$ (min)
PLLA	90	22.31		2.60	1.66×10^{-3}	0.99998	10.23	10.18
	100	22.60		2.51	3.16×10^{-2}	0.99994	3.47	3.42
	110	32.95		2.67	2.51×10^{-2}	0.99988	3.51	3.46
	114	33.48		2.60	1.51×10^{-2}	1.00000	4.33	4.35
	116	36.97		2.59	1.26×10^{-2}	0.99998	4.63	4.70
	118	35.78		2.73	7.59×10^{-3}	1.00000	5.20	5.23
	120	42.28		2.80	5.25×10^{-3}	1.00000	5.65	5.72
	130	53.44		2.83	1.82×10^{-4}	0.99982	17.83	18.42
	140	51.34		2.91	7.94×10^{-6}	0.99994	48.67	49.87
PLLA/CHAp	90	19.38	21.53	2.43	8.32×10^{-3}	0.99996	6.30	6.17
	100	22.27	24.74	2.47	1.15×10^{-1}	0.99998	2.10	2.07
	110	23.30	25.89	2.42	1.10×10^{-1}	0.99996	2.12	2.14
	114	27.88	30.98	2.52	4.90×10^{-2}	0.99996	2.83	2.86
	116	29.12	32.36	2.51	4.27×10^{-2}	0.99998	2.98	3.04
	118	30.94	34.38	2.57	3.10×10^{-2}	0.99994	3.30	3.35
	120	31.91	35.46	2.72	1.95×10^{-2}	1.00000	3.68	3.72
	130	37.23	41.37	2.83	2.29×10^{-3}	1.00000	7.55	7.53
	140	38.06	42.29	2.86	1.66×10^{-4}	0.99996	18.35	18.45

ΔH_c^* : denotes the crystallization enthalpy normalized to unit mass of PLLA.
r^2: denotes the coefficient of determination for the Avrami fit.
$t_{0.5}^*$: denotes the half-life crystallization time obtained from the experiment (symbols in Fig. 4).
$t_{0.5}$: denotes the half-life crystallization time calculated by eq. (7).

be either 0 or 1, where 0 corresponds to instantaneous or heterogeneous nucleation and 1 to sporadic or homogenous nucleation. However, because in many cases the nucleation may be somewhere between completely instantaneous and completely sporadic nucleation, a noninteger Avrami exponent can be sometimes explained in this way.[20] The Avrami n for neat PLLA is from 2.6 to 2.9 in the isothermal temperature range of 90–140°C. the Avrami n for PLLA/CHAp is from 2.4 to 2.9 in the same temperature range. The Avrami exponent close to 3 at high isothermal crystallization temperatures indicates a changing trend of PLLA crystal growth from two- to three-dimensional with instantaneous nucleation and athermal.[5] The obtained n values were similar to those reported for neat PLLA (2.4–3.2 at T_c = 90–125°C by Tsuji et al.,[22] 2.8–3.2 at T_c = 90–130°C by Iannace and Nicolais,[5] 2.5–3.3 at T_c = 90–130°C by Kolstad[23]). However, Miyata and Masuko[6] reported an n value of about 4 at T_c = 110–132.5°C. The differences can be attributed to the determination of the onset of crystallization or induction time, the establishment of the baseline and incomplete isothermal crystallization data, the effect of the cooling rate from the melt to the isothermal crystallization temperature and the relative degree of crystallinity range employed for the Avrami fitting.[20] Also, the nucleation is seldom either athermal or simple thermal.[24] It can be seen from Table II that the values of Avrami exponent (n) of the PLLA/CHAp nanocomposite are lower than those of the neat PLLA for the same crystallization temperatures. One possible reason is that the large amount of CHAp nanoparticles might have affected the nucleation and growth mechanisms of the PLLA crystals. Better interpretation of the Avrami exponent requires more information about the specific nucleation and growth mechanisms of PLLA crystal, but at this stage we do not have such information.

The half-life crystallization time $t_{0.5}$, which is defined as the time at $X_t = 0.5$, is an important parameter for the discussion of crystallization kinetics. It can also be calculated using the equation:

$$t_{0.5} = \left(\frac{\ln 2}{k}\right)^{1/n} \tag{7}$$

The half-life crystallization time $t_{0.5}$ can be either obtained directly from the curve of relative degree of crystallinity with time (Fig. 4) or calculated from isothermal parameter n and k by using eq. (7). These two sets of data are compared in Table II. They are very close to each other for both neat PLLA and PLLA/CHAp within the range of crystallization temperatures. The value of $1/t_{0.5}$ can be used to describe the crystallization rate and is plotted in Figure 5 as a function of isothermal crystallization temperature. As a typical semicrystalline polymer, the crystallization of PLLA is slow in temperature ranges close to the melting point and glass transition point. Di Lorenzo[7] reported a discontinuity around 116–118°C in a similar plot, which was ascribed to a

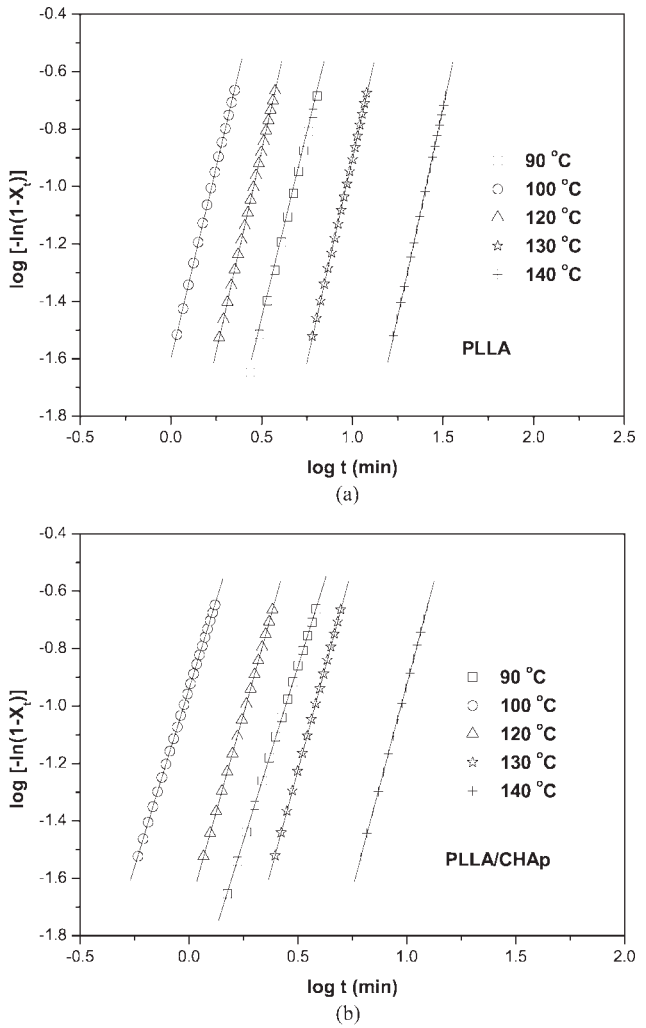

Figure 3 Avrami plots for isothermal crystallization of (a) neat PLLA and (b) PLLA/CHAp nanocomposite (Symbols: experimental data; solid lines: Avrami linear fit).

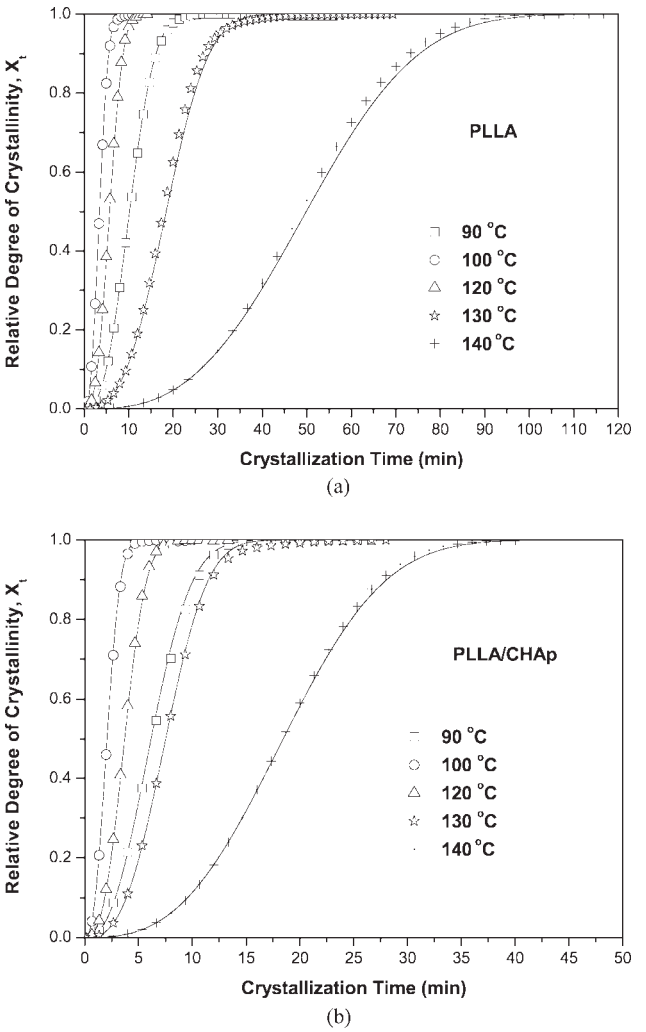

Figure 4 Development of relative degree of crystallinity as a function of crystallization time for (a) PLLA and (b) PLLA/CHAp nanocomposite (Symbols: experimental data; solid lines: calculated crystallinity using eq. (2) and Avrami parameters n and k in Table II).

sudden acceleration in spherulite growth. However, such discontinuity is not clear in Figure 5. It can be seen that the crystallization rate of PLLA/CHAp was faster than neat PLLA. This implies that the nanosized CHAp particles acted as an efficient nucleating agent. The highest overall isothermal crystallization rate was found between 100 and 110°C. The increased crystallization rate due to the addition of CHAp into PLLA matrix was also confirmed by the higher values of isothermal crystallization parameter k listed in Table II. Similar observations of inorganic particle reinforced PLLA composites exhibited increased bulk crystallization rates relative to neat polymer.[18,25] This phenomenon is usually attributed to the higher heterogeneous nucleation rates, as demonstrated by increases in the isothermal crystallization parameter k. However, the effects of inorganic fillers on radial spherulite growth rates vary, depending on the properties and content of the fillers.

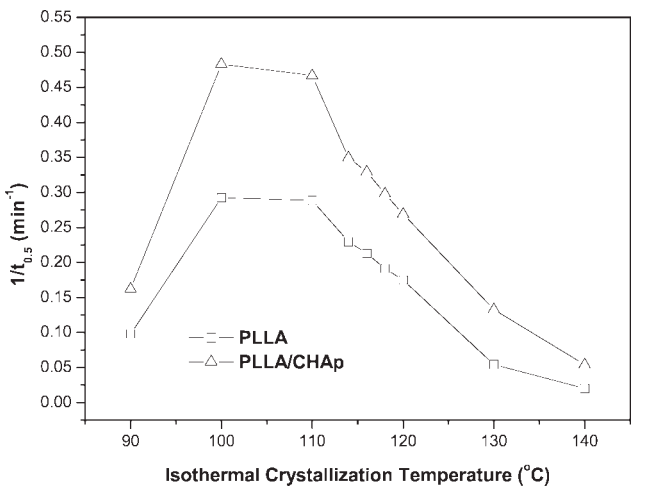

Figure 5 Dependence of $1/t_{0.5}$ of PLLA and PLLA/CHAp nanocomposite on isothermal crystallization temperature.

Crystal growth analysis by LH theory

The isothermal crystallization data obtained can be examined in terms of secondary nucleation or LH theory of polymer crystal growth.[26] The growth face undergoes two different but related processes during polymer crystallization. One is the deposition of secondary nuclei on the growth face, and the other is the subsequent growth along the face at the sites where the secondary nuclei are formed. Therefore, there are two competing rates involved in the process that determine the regime in which the polymer crystallizes. On the basis of the secondary nuclei formation rate, i, and the lateral growth rate or the surface spreading rate, g, the crystallization regimes can be defined as follows:

$$i \ll g \quad \text{Regime I}$$

$$i \sim g \quad \text{Regime II}$$

$$i \gg g \quad \text{Regime III}$$

Regime I, where i is much smaller than g, occurs at very low supercoolings (ΔT); Regime II, where i is in the order of g, occurs at moderate ΔT; and Regime III, where i is much greater than g, occurs at very high ΔT.[27] Thus Regime I is characterized by mononucleation of the nucleus on a substrate, followed by lateral spreading or growth of a chain-folded crystal lamella. The linear growth rate is controlled by secondary nucleation in Regime I. In contrast, Regime II occurs by multiple nucleations at lower crystallization temperatures.[28] As the temperature is further lowered, prolific and multiple nucleation can occur in Regime III.[24] Most polymers exhibit different regime behavior, depending on the crystallization condition.

LH theory assumes that a free energy barrier associated with nucleation has an energetic origin and it provides the general expression for the growth rate (G) of a linear polymer crystal with folded chains:

$$G = G_0 \exp\left[\frac{U}{R(T_c - T_\infty)}\right] \exp\left(\frac{-K_g}{T_c \Delta T f}\right) \qquad (8)$$

where K_g is the nucleation constant [for details see eq. (11)]; ΔT is the undercooling defined by $T_m^0 - T_c$; T_m^0 is the equilibrium melting point which is 479.2K[5] for PLLA; f is a factor given as $2T_c/(T_m^0 + T_c)$; U is the activation energy for polymer diffusion, which means the transportation of segments to the crystallization site, and the universal value of $U = 1500$ cal/mol (6276 J/mol) was used to compare the results from literature[5]; R is the gas constant [8.314 J/(mol K)]; T_∞ is the hypothetical temperature where all motion associated with viscous flow ceases and normally chosen as T_g-30 K; and G_0 is the front factor.

Using a theoretical approach, it can be shown that the linear growth rate G can be considered proportional to $1/t_{0.5}$. Based on the LH theory,[29] the temperature variation of $1/t_{0.5}$ can be written as:

$$\left(\frac{1}{t_{0.5}}\right) = \left(\frac{1}{t_{0.5}}\right)_0 \exp\left[\frac{U}{R(T_c - T_\infty)}\right] \exp\left(\frac{-K_g}{T_c \Delta T f}\right) \qquad (9)$$

It should be pointed out that this is only an approximation. Ideally, the value of spherulite growth rate (G) should be measured directly by optical microscopy and eq. (8) be applied. However, the spherulites of the PLLA/CHAp nanocomposite were too small and accurate measurements of their growth rate were not possible. Second, the G values measured by optical microscopy are obtained under a confined 2D environment, i.e., the spherulites will grow between two microscope cover slides. Also, there is doubt whether limited number of 2D measurements can really represent the true 3D spherulite growth in large number. On the other hand, DSC analysis allows 3D polymer spherulite growth and the data will give a more macroscale representation of the real situation.

For practical convenient use, eq. (9) is usually rewritten as:

$$\ln\left(\frac{1}{t_{0.5}}\right) + \frac{U}{R(T_c - T_\infty)} = \ln\left(\frac{1}{t_{0.5}}\right)_0 - \frac{K_g}{T_c \Delta T f} \qquad (10)$$

The plot of the left-hand side of eq. (10) vs. $1/T_c \Delta T f$ gives the slope of $-K_g$ from which the nucleation constant K_g can be evaluated. In the current investigation, $U = 6276$ J/mol, as stated earlier, was used in the plot (Fig. 6). For both neat PLLA and PLLA/CHAp, there were two crystallization

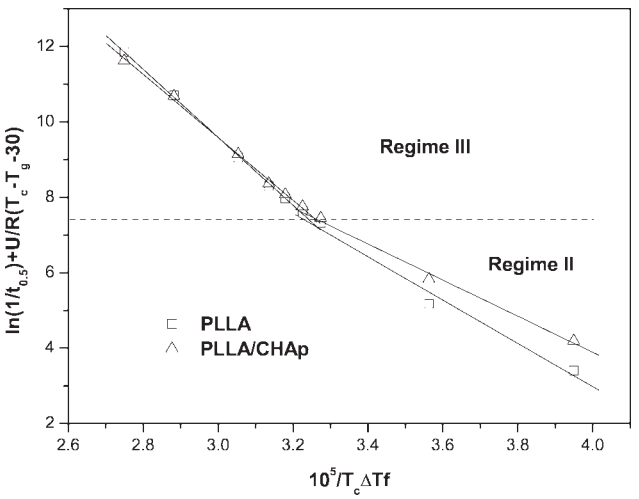

Figure 6 Hoffman-Lauritzen plots for the estimation of nucleation parameters of neat PLLA and PLLA/CHAp nanocomposite (Symbols: the data calculated from isothermal crystallization kinetic parameters; solid lines: the Lauritzen-Hoffman linear fitting curves).

TABLE III
Lauritzen-Hoffman Parameters for Isothermal Crystallization of Neat PLLA and PLLA/CHAp Nanocomposite

Samples	K_g (III) (K^2)	σ_e (III) (J/m^2)	q (III) (kJ/mol)	K_g (II) (K^2)	σ_e (II) (J/m^2)	q (II) (kJ/mol)
PLLA	9.02×10^5	91×10^{-3}	33.8	5.74×10^5	117×10^{-3}	43.5
PLLA/CHAp	8.36×10^5	84×10^{-3}	31.2	4.79×10^5	96×10^{-3}	35.7

regimes, i.e., Regimes II and III, in the isothermal temperature range. From Figure 6, the K_g (II) values for neat PLLA and PLLA/CHAp were estimated to be 5.74×10^5 K^2 and 4.76×10^5 K^2, respectively, within the T_c range of 120–140°C (Table III). The K_g (II) value for neat PLLA was higher than those reported in the literature, including 2.92×10^5 based on isothermal crystallization parameters[5] and 3.01×10^5 on spherulite growth rate G values.[22] K_g (III) for neat PLLA obtained here was 9.02×10^5, which was similar to 8.91×10^5 as reported by Iannace and Nicolais[5] and 9.00×10^5 by Tsuji et al.[22] According to Iannace and Nicolais,[5] the theoretical value of the ratio K_g (III)/K_g (II) is 2. In the current investigation, the respective ratios for neat PLLA and PLLA/CHAp were 1.57 and 1.74. The lower values obtained here could be related to either the different sets of values utilized for U and T_∞ or the difference in molecular weight of polymers used.

The transition from Regime II to Regime III was observed at about 120°C for both neat PLLA and PLLA/CHAp, which was in agreement with the results obtained using G values.[5,22,30,31] This indicates that the LH theory is a valid method to predict nucleation constant if the Avrami fit is good. The current investigation shows that the addition of CHAp nanoparticles did not alter the transition temperature of PLLA crystallization from Regime II to Regime III but caused a reduction in the value of K_g. The lower K_g for PLLA/CHAp suggests that less energy was needed for the formation of critical size of PLLA nuclei in the nanocomposite than in the neat PLLA.

The nucleation constant K_g in eq. (8) is given by:

$$K_g = \frac{Zb_0\sigma\sigma_e T_m^0}{\Delta h_f k_B} \tag{11}$$

where σ is the lateral surface free energy, σ_e is the fold surface energy, b_0 is the layer thickness of the crystal, Δh_f is the volumetric heat of fusion, and k_B is the Boltzmann constant. The value of Z is dependent on the crystallization regime and equal to 4 for Regimes I (high temperatures) and III (low temperatures) and values 2 for Regime II (intermediate temperatures).[7] In the current investigation, the K_g values were used to calculate the fold surface free energy according to eq. (11). The lateral surface energy was determined by the Thomas-Stavely empirical equation[26]:

$$\sigma = \alpha_0 \Delta h_f \sqrt{a_0 b_0} \tag{12}$$

where α_0 is an empirical constant and usually assumed to be 0.25, which is appropriate to high melting polyesters[32]; $a_0 b_0$ represents the cross-sectional area of PLLA chains, with $a_0 = 5.97 \times 10^{-10}$ m and $b_0 = 5.17 \times 10^{-10}$ m from the literature; and $\Delta h_f = 1.11 \times 10^{-8}$ J/m^3.[33] The σ value was then calculated to be 15.4×10^{-3} J/m^2, which was close to the reported data.[25] The values of fold surface energy σ_e were obtained by solving eq. (11) and are listed in Table III. For neat PLLA, the value of σ_e varies in the range of 91–117 erg/cm^2 (1 erg/cm^2 = 1×10^{-3} J/m^2), which agrees well with the result (107 erg/cm^2) by Miyata and Masuko[6] but higher than 40.5 erg/cm^2 by Di Lorenzo[33] and 43.5 erg/cm^2 by Wu et al.[18] It has been shown that the value of σ_e is dependent on the molecular weight of PLLA[6] and the cooling or heating rate to the isothermal crystallization temperature.[18] Miyata and Masuko[6] implied that the value of σ_e increases with increase in the loose-loop chains on the fold surface of high molecular weight PLLA. The decrease of σ_e with increasing heating rate was considered by Wu et al.[18] due to the change of nucleation mechanism from Regime III to Regime II by LH–Miller analysis. However, they did not show the transition temperature from Regime III to Regime II.

It can be seen from Table III that addition of CHAp nanoparticles decreased the values of σ_e for PLLA by 18% in Regime II and 7.7% in Regime III. The lower values of the free energy of chain folding of the lamellar crystals in PLLA/CHAp suggest that the CHAp nanoparticles facilitated the crystallization of PLLA. According to Wittmann and Lotz,[34] the incorporation of nucleating agents into polymers changes the polymer crystallization behavior. Heterogeneous nucleating agents, such as filler particles and fibers, tend to promote the nucleation of spherulites on their surfaces, decrease the lamellar thickness, and lead to epitaxial growth of crystallites. In this study, the nucleating ability of the CHAp has been clearly shown in Figure 7, but the latter two mechanisms have not been examined.

Finally, the work for chain folding, q, which means by bending the polymer chain back upon itself in the appropriate configuration and is apparently correlated with molecular structure, can be expressed as follows[27]:

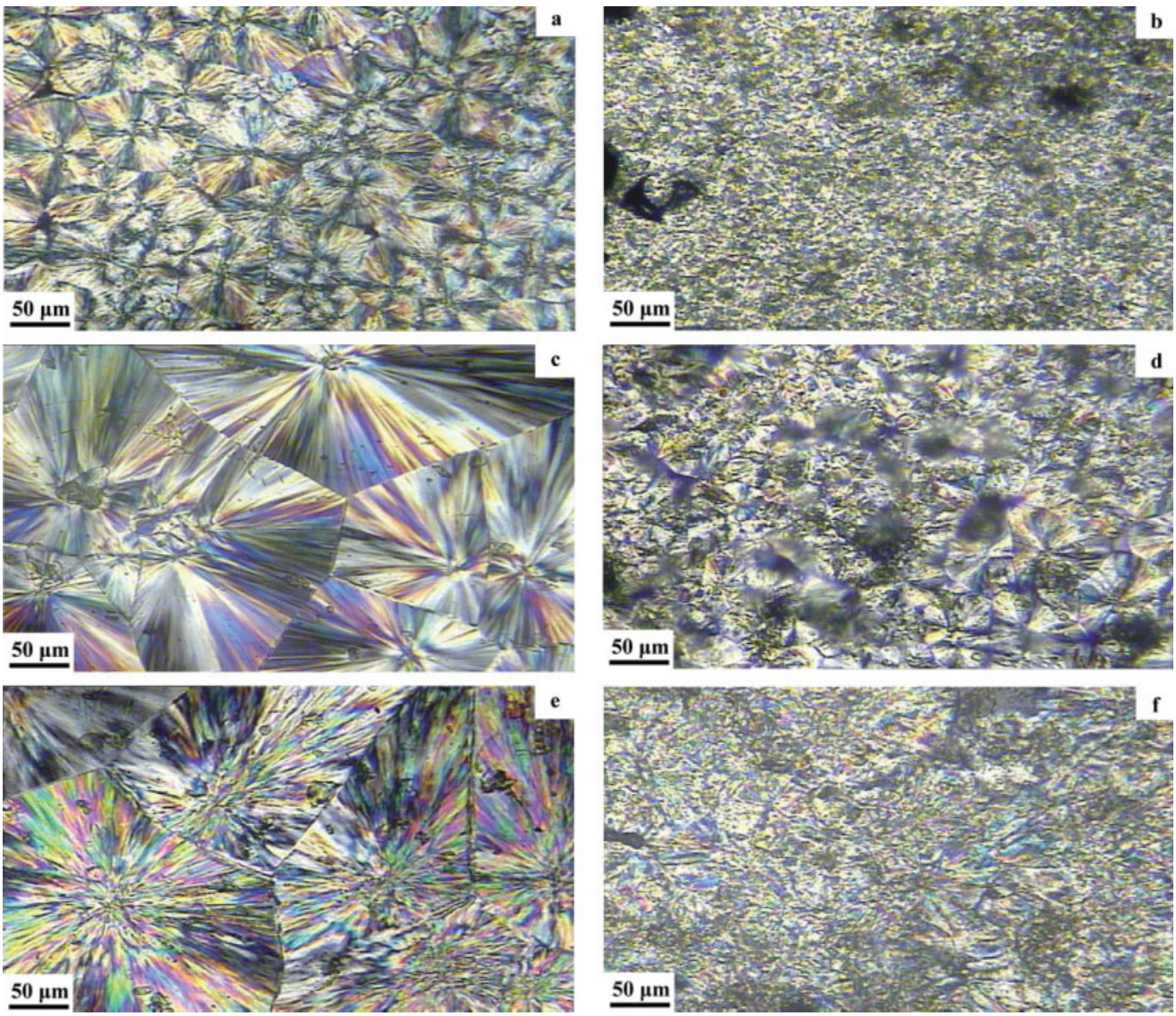

Figure 7 Polarized optical micrographs showing the spherulitic morphologies of neat PLLA and PLLA/CHAp crystallized at various temperatures: (a) neat PLLA at 110°C for 50 min, (b) PLLA/CHAp at 100°C for 30 min, (c) neat PLLA at 120°C for 90 min, (d) PLLA/CHAp at 120°C for 40 min, (e) neat PLLA at 130°C for 180 min, and (f) PLLA/CHAp at 130°C for 70 min. [Color figure can be viewed in the online issue, which is available at www.interscience.wiley.com.]

$$q = 2a_0 b_0 \sigma_e \tag{13}$$

The values of q in Regime II and Regime III for neat PLLA and PLLA/CHAp nanocomposite were determined and are listed in Table III. It was found that the values of q for neat PLLA were higher than those for PLLA/CHAp in both Regime II and Regime III. q is a measure of the inherent stiffness of polymer chain: more flexible chains have smaller values of q, and vice versa.[35] The results show that the CHAp nanoparticles reduced the work needed for PLLA chains to fold into the crystal. Such phenomenon may arise due to a reduced size or a lower degree of perfection of the crystals formed.

Spherulite morphology

The spherulitic morphologies of neat PLLA and PLLA/CHAp nanocomposite were investigated using polarized optical microscopy at selected crystallization temperatures of 110, 120, and 130°C, and the results are shown in Figure 7(a–f). Because sufficient time was given for crystallization, according to the isothermal crystallization kinetics study, both neat PLLA and PLLA/CHAp were completely crystallized. It can be seen from Figure 7 that the spherulites of neat PLLA were distinctive and of considerable size, whereas those of PLLA/CHAp were much smaller and less distinctive. This clearly shows that the nanosized CHAp acted as an

effective nucleating agent to induce a great number of additional nuclei, but, on the other hand, it also limited the growth space for each nucleus, leading to the formation of smaller spherulites. In the theoretical approach for growth rate analysis, the LH equation can be applied using half-time of crystallization ($t_{0.5}$) under the assumption that the crystallization rates are inversely proportional to $t_{0.5}$. This theoretical approach has been widely used in crystallization study of both neat polymers and their composite systems.[5,18,22,36,37] It is shown in Figure 5 that the values of $1/t_{0.5}$ for the PLLA/CHAp nanocomposite were higher than those of the neat PLLA, which means the nanocomposite has a higher crystallization rate than the neat polymer.

Nonisothermal crystallization kinetics

The nonisothermal crystallization thermograms for neat PLLA and PLLA/CHAp nanocomposites obtained at six cooling rates are shown in Figure 8. From these curves, useful crystallization parameters such as the peak temperature (T_p), at which the sample has the fastest crystallization, can be determined and used for further calculations. It can be seen that the crystallization enthalpy first increased and then decreased with increasing cooling rates. This phenomenon was also reported by Chen et al.[38] in the nonisothermal crystallization study of maleated poly(3-hydroxybutyrate). The crystallization enthalpy reached a maximum at about 2.5°C/min for neat PLLA and 5°C/min for PLLA/CHAp is caused by crystallization in the α' polymorph, that causes a drastic increase of crystallization rate below 120°C.

Ozawa[39] extended the Avrami equation for the nonisothermal crystallization analysis. Assuming that the nonisothermal crystallization process is composed of infinitesimally small isothermal crystallization steps, the relative volumetric crystallinity X_t at temperature T can be calculated as follows:

$$X_t = 1 - \exp\left[\frac{-K(T)}{\phi^m}\right] \tag{14}$$

or

$$\log[-\ln(1 - X_t)] = \log K(T) + m \log \phi^{-1} \tag{15}$$

where m is the Ozawa exponent, which depends on the dimensions of the crystal growth, and $K(T)$ is a function of cooling rate ϕ and indicates how fast crystallization occurs. If the Ozawa method is valid, plots of log $[-\ln (1 - X_t)]$ versus log ϕ^{-1} should be straight lines, and kinetic parameters $K(T)$ and m should be obtainable from the intercept and slope of the lines, respectively. However, when the cooling rates vary in a large range, the poor linearity of the plots renders the results calculated from eq. (14)

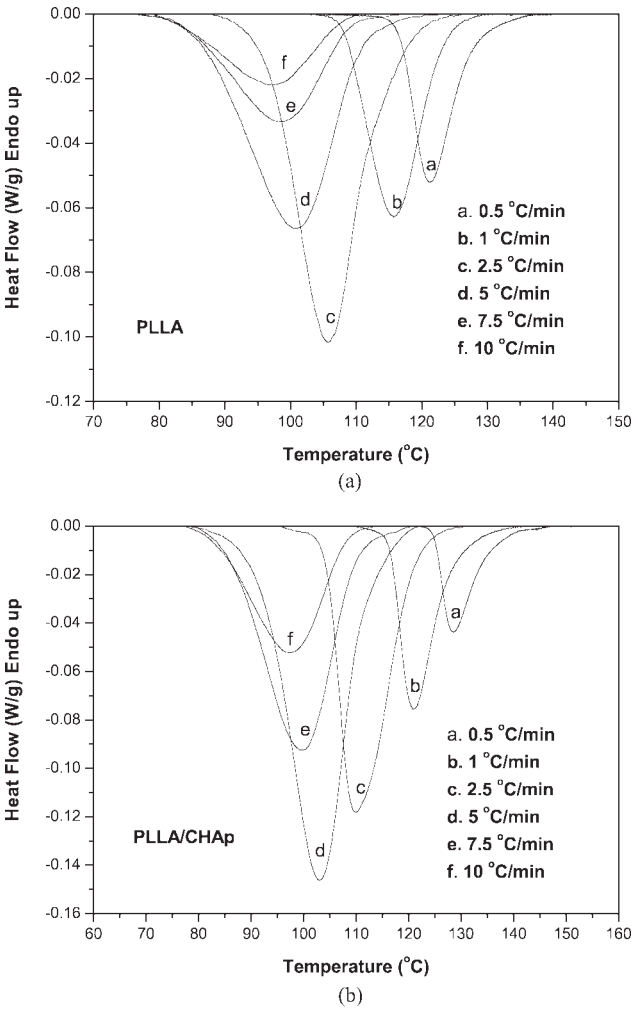

Figure 8 DSC thermograms obtained from nonisothermal crystallization of (a) neat PLLA, and (b) PLLA/CHAp nanocomposites (Cooling rates are indicated in the graphs).

questionable. Moreover, the assumption of constant cooling rates may cause problems in modeling the change of crystallinity during polymer processing.[40] The Ozawa theory neglects the slow secondary crystallization and the dependence of lamellar thickness on the temperature so that it cannot describe the full process of nonisothermal crystallization of polymers in general.[18,40–43]

Aiming to find a method to describe exactly the nonisothermal crystallization process, a combination of Avrami and Ozawa equations was proposed recently.[44] During the nonisothermal crystallization process, the relationship between crystallization time t and temperature T is given by

$$t = \frac{T_0 - T}{|\phi|} \tag{16}$$

where T is the temperature at time t, T_0 is the initial temperature when crystallization begins ($t = 0$). The

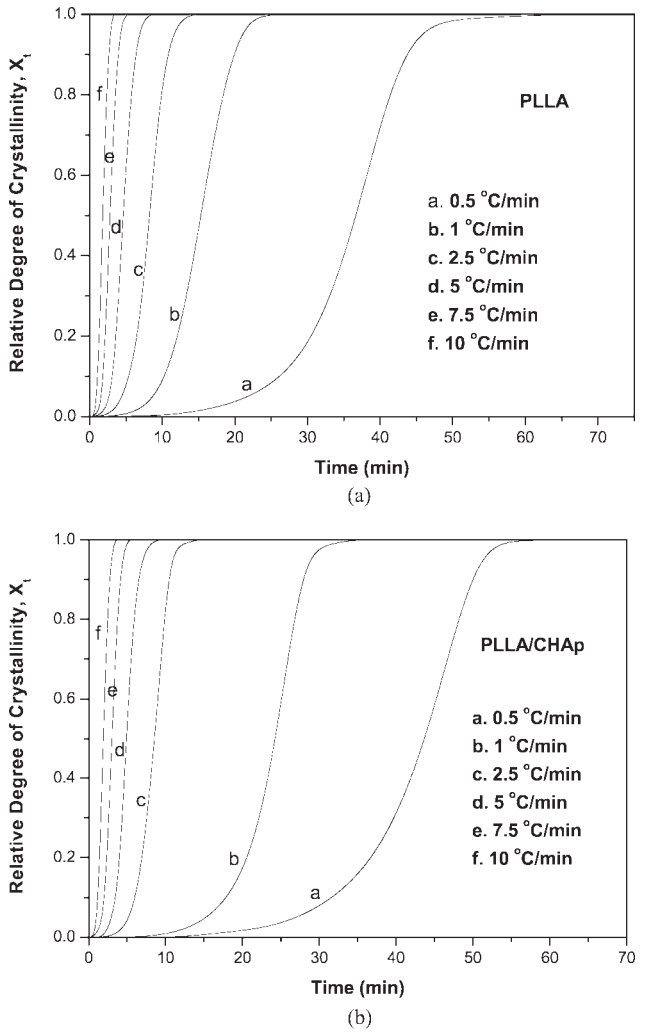

Figure 9 Plots of relative degree of crystallinity as a function of time for (a) neat PLLA, and (b) PLLA/CHAp nanocomposite (Materials were crystallized nonisothermally at various cooling rates).

Avrami equation relates X_t with time t, and the Ozawa equation relates X_t with cooling rate ϕ, thus the relationship between ϕ and t can be established to connect these two equations as follows:

$$\log \phi = \log F(T) - \alpha \log t \tag{17}$$

where the rate parameter $F(T) = [\frac{K(T)}{k}]^{1/m}$ and the physical meaning is the necessary value of cooling rate to reach a defined degree of crystallinity at unit crystallization time; α is the ratio of the Avrami exponent n to the Ozawa exponent m, i.e., $\alpha = n/m$. According to eq. (17), at a given degree of crystallinity, the plot of $\log \phi$ as a function of $\log t$ gives a straight line with $\log F(T)$ as the intercept and $-\alpha$ as the slope. The combined Ozawa-Avrami model actually is a modified model in which crystallization functions are related to certain X_t values. This method is more convenient in the analysis of nonisothermal crystallization process, but it needs to be considered with care about its physical meaning.[45]

Figure 9 presents the relative degree of crystallinity as a function of time for neat PLLA and PLLA/CHAp crystallized at various cooling rates. The higher the cooling rate, the shorter the time range within which crystallization occurs. The retardation effect of cooling rate on the crystallization is observed only at low cooling rates (<5°C/min), below which the $X_t - t$ curve shows an obvious S shape. At higher cooling rates, melted PLLA evolves into the glassy state quickly and hence the $X_t - t$ curve tends to straight.

Figure 10 presents the plots of $\log \phi$ as a function of $\log t$ for neat PLLA and PLLA/CHAp. The good linearity of the plots demonstrates the good applicability of the combined Avrami-Ozawa method in the current investigation. Values of $F(T)$ and α are listed in Table IV, from which it can be seen that the

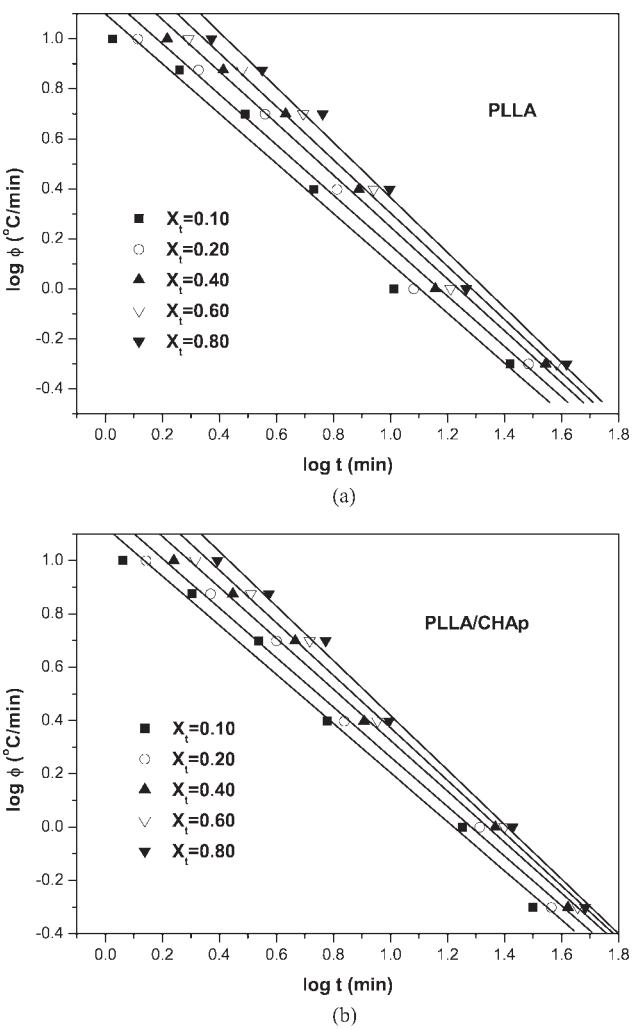

Figure 10 Plots of $\log \phi$ as a function of $\log t$ for (a) neat PLLA and (b) PLLA/CHAp nanocomposite (based on combined Ozawa-Avrami equation).

TABLE IV
Values of *F(T)* and α Obtained from the Combined Avrami-Ozawa Equation for Neat PLLA and PLLA/CHAp Nanocomposite

	PLLA			PLLA/CHAp		
X_t	α	$F(T)$	r^2	α	$F(T)$	r^2
0.10	1.00	12.59	0.9820	0.92	13.49	0.9898
0.20	1.01	15.14	0.9837	0.93	15.49	0.9917
0.40	1.04	19.50	0.9867	0.96	19.06	0.9940
0.60	1.06	23.44	0.9880	0.99	22.91	0.9951
0.80	1.10	29.51	0.9887	1.02	27.54	0.9956

r^2 denotes the coefficient of determination of Figure 10.

values of $F(T)$ increase systematically with an increase in the relative degree of crystallinity. Thus, at a unit crystallization time, a higher cooling rate is needed to achieve a higher degree of crystallinity. $F(T)$ is considered as a parameter that indicates the polymer crystallization rate. A lower $F(T)$ value means a higher crystallization rate under nonisothermal crystallization condition.[46] The PLLA/CHAp nanocomposite had a larger $F(T)$ value than neat PLLA in the low X_t range (<0.40), whereas the trend was opposite in the high X_t range (≥0.40). This indicates that the addition of CHAp only accelerated the PLLA crystallization rate in the initial crystallization stage. The values of parameter α are nearly constant and close to 1 which means that the Avrami exponent and Ozawa exponent are more or less the same for both neat PLLA and PLLA/CHAp.

Effective activation energy of nonisothermal crystallization

The crystallization activation energy during nonisothermal processes for neat PLLA and PLLA/CHAp can be evaluated using the Kissinger equation[47]:

$$\frac{d[\ln(\phi/T_p^2)]}{d(1/T_p)} = -\frac{\Delta E_C}{R} \tag{18}$$

where ΔE_C is the crystallization activation energy, and R is the gas constant. The activation energy ΔE_C can be obtained from the slope of the plot of $\ln(\phi/T_p^2)$ versus $1/T_p$, which is presented in Figure 11 for neat PLLA and PLLA/CHAp, respectively. The calculated ΔE_C for neat PLLA and PLLA/CHAp are –149.67 and –124.91 kJ/mol, respectively. ΔE_C values are negative, indicating that the rate of crystallization increased with decreasing temperature, and the crystallization process of polymer is a barrierless and spontaneous process (the lower the value of ΔE_C the faster is the crystallization rate).[48] The obtained crystallization activation energy of neat PLLA fits well with the reported value of –146.86 kJ/mol.[49]

There are other methods for obtaining the activation energy from nonisothermal crystallization, such as the Augis-Bennett method[50] and the Takhor method.[51] But the Kissinger method appears to be the most popular method for evaluating ΔE_C. However, all these three methods involve the cooling rate ϕ but its negative sign has been omitted in the logarithm formulation. Recently, Vyazovkin[52] demonstrated that dropping the negative sign for ϕ is a mathematically invalid procedure that generally makes the Kissinger-type equation inapplicable to melt crystallization. Another disadvantage is that only a single value of activation energy is used for multiple nonisothermal crystallization processes by Kissinger-type methods. However, the crystallization rate is determined by the rates of nucleation and growth, whose activation energies are likely to be different. To overcome the disadvantages of Kissinger-type methods, an isoconversion method can be applied to nonisothermal crystallization for evaluating the dependence of the activation energy on crystallinity and temperature. The representative methods include the differential isoconversion method[53] and the advanced integral isoconversion method.[54] In the current investigation, the numerical differential method by Friedman[53] was used. According to Friedman, different effective activation energies are calculated for every degree of crystallinity using the following equation:

$$\ln\left(\frac{dX}{dt}\right)_{X,i} = Const - \frac{\Delta E_X}{RT_{X,i}} \tag{19}$$

where dX/dt is the instantaneous crystallization rate as a function of time at a given crystallinity X, ΔE_X is the effective activation energy at given crystallinity X, $T_{X,i}$ is the set of temperatures related to a given crystallinity X at different cooling rates and

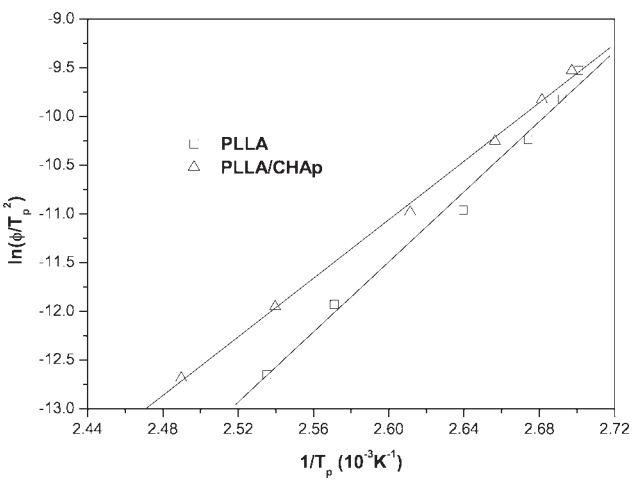

Figure 11 Plots of ln (ϕ/T_p^2) as a function of $1/T_p$ for neat PLLA and PLLA/CHAp nanocomposite.

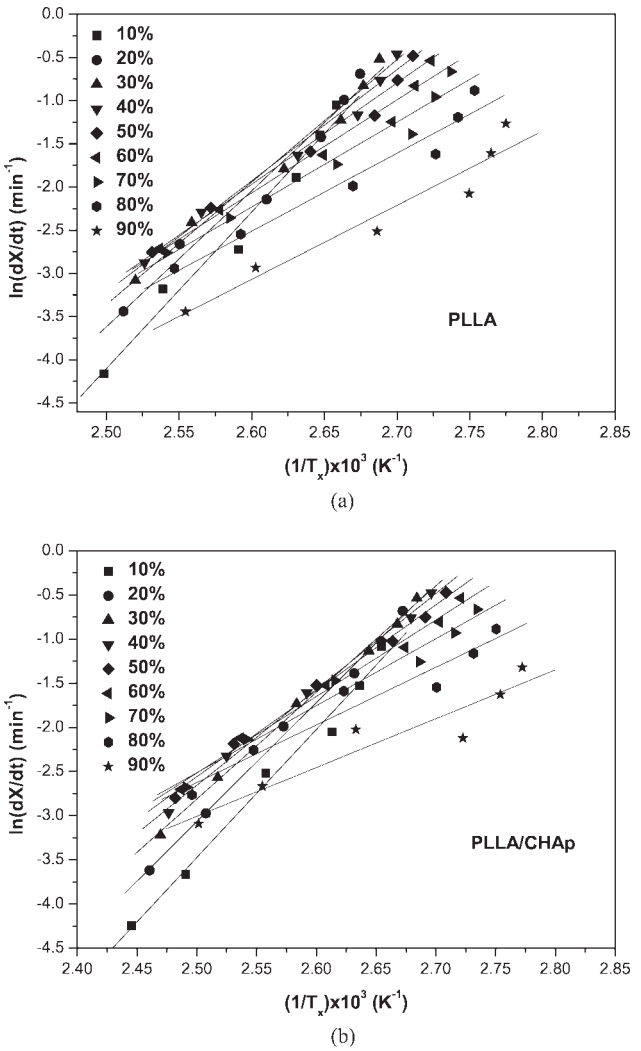

Figure 12 Friedman plots of ln(dX/dt) vs. $1/T_x$ for (a) neat PLLA and (b) PLLA/CHAp nanocomposite at different relative degrees of crystallinity (The solid lines represent the linear fits).

the subscript i refers to every individual cooling rate used. The instantaneous crystallization rate, dX/dt, can be obtained from Figure 9 by differentiation. Furthermore, by selecting appropriate degrees of crystallinity (i.e., from 10 to 90%) the values of dX/dt at a specific X are correlated to the corresponding crystallization temperature, T_X. Then by plotting dX/dt with respect to $1/T_X$, a straight line should be obtained with a slope equal to $\Delta E_X/R$.

Figure 12 shows Friedman plots for neat PLLA and PLLA/CHAp nanocomposites at different relative degrees of crystallinity. The straight lines obtained were used to calculate the effective activation energies of neat PLLA and PLLA/CHAp, which are shown in Figure 13. As can be seen, the effective activation energy increased with the increase in the relative degree of crystallinity for all neat PLLA and PLLA/CHAp. In all cases, the absolute values of

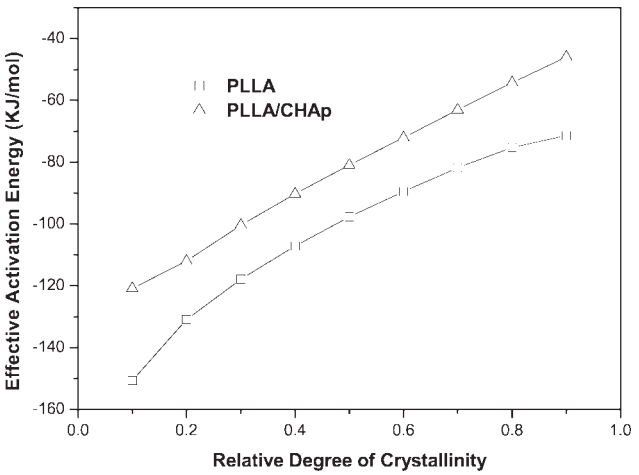

Figure 13 Dependence of effective activation energy on relative degree of crystallinity in nonisothermal crystallization of neat PLLA and PLLA/CHAp nanocomposite.

ΔE_X for PLLA was higher than that for PLLA/CHAp, indicating that the CHAp nanoparticles (10 wt%) lower the nonisothermal crystallization rate of PLLA. Interestingly, the values of activation energy obtained by the Kissinger method for both PLLA and PLLA/CHAp also fall on the curves in Figure 13 at the relative degree of crystallinity near 10%. This indicates that the Kissinger method may represent one case in the ΔE_X dependence of crystallinity by the Friedman method.

Furthermore, the relative degree of crystallinity is dependent on the nonisothermal crystallization temperature. Thus, the effective activation energy can be plotted as a function of temperature by taking an average crystallization temperature associated with a

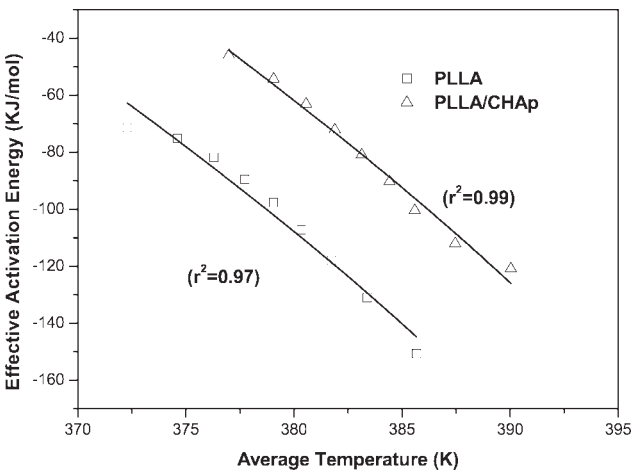

Figure 14 Dependence of effective activation energy on average temperature for neat PLLA and PLLA/CHAp nanocomposite. (The solid lines represent the nonlinear fits.)

TABLE V
Lauritzen-Hoffman Parameters for Neat PLLA and PLLA/CHAp Nanocomposite Obtained Through Isoconversion Analysis of their Nonisothermal Crystallization

Samples	U (J/mol)	K_g (III) (K^2)	Coefficient of determination, r^2
PLLA	1846	7.52×10^5	0.97
PLLA/CHAp	2565	6.37×10^5	0.99

certain relative degree of crystallinity.[55] The symbols in Figure 14 display the $\Delta E_X - T$ relationship for neat PLLA and PLLA/CHAp, respectively. Vyazovkin and Sbirrazzuoli[56] recently derived an equation to correlate the dependence of effective activation energy on temperature in terms of the LH parameters (U and K_g):

$$E_X(T) = U\frac{T^2}{(T - T_\infty)^2} + K_g R\frac{T_m^{0^2} - T^2 - T_m^0 T}{(T_m^0 - T)^2 T} \quad (20)$$

In the current investigation, the graphics software Origin® (Microcal Software, Inc.) was employed to perform the nonlinear fits of eq. (20), and the results are shown as the solid lines in Figure 14. The values of T_∞ and T_m^0 used were the same as those in Crystal growth analysis by LH theory section. The values of U and K_g yielded by the fits are shown in Table V. The coefficients of determination (r^2) were found to be 0.97 and 0.99 for neat PLLA and PLLA/CHAp, respectively. The K_g values were similar to the values obtained from the isothermal crystallization analysis for Regime III, i.e., for crystallization temperatures below 120°C (refer to Crystal growth analysis by LH theory section). However, the regime transition was not observed due to the limited temperature intervals in the nonisothermal crystallization experiment. The obtained values of U were much lower than the commonly used value of 6276 kJ/mol. This indicates that the commonly used value of U may not be applicable to all polymers. The current analysis has demonstrated that the parameters of the LH equation can be obtained from DSC data on the overall rates of nonisothermal crystallization. In fact, this method have been successfully applied to the nonisothermal crystallization of a poly(ethylene terephthalate) with medium to slow crystallization rates by Vyazovkin and Sbirrazzuoli,[56] poly(propylene terephthalate) and poly(butylene 2,6-naphthalate) with fast crystallization rates by Achilias et al.[57] and nanocomposites of polyamide 6/halloysite nanotube recently by Guo et al.[58] In the current investigation, the validity of using the Vyazovkin-Sbirrazzuoli method for PLLA and PLLA/CHAp nanocomposite has been demonstrated.

CONCLUSIONS

The following conclusions can be drawn from the investigation into the effects of inclusion of CHAp nanoparticles on thermal properties, isothermal, and nonisothermal melt crystallization kinetics of PLLA:

1. The addition of 10 wt% of CHAp decreased the glass transition temperature and cold crystallization temperature of PLLA and slightly increased the melting temperature of PLLA. When cooled rapidly (50°C/min) from the melt, the neat PLLA remained amorphous, whereas PLLA/CHAp exhibited a crystallinity of 4%, which was probably caused by induced heterogeneous nucleation due to the presence of CHAp nanoparticles.
2. At high-isothermal crystallization temperatures, the addition of CHAp decreased the crystallization enthalpy significantly compared with that of neat PLLA. Such changes imply a drop in the amount of crystals formed or a lower degree of perfection of the crystals. The Avrami equation described the isothermal crystallization kinetics well for both neat PLLA and PLLA/CHAp. The Avrami exponent n for neat PLLA and PLLA/CHAp approached 3 when increasing the isothermal crystallization temperature to 140°C, which indicates a three-dimensional crystal growth. The maximum isothermal crystallization rate was found to be between 100 and 110°C.
3. By using LH theory, the nucleation constant (K_g), the fold surface energy (σ_e), and the work of chain folding (q) for neat PLLA and PLLA/CHAp could be obtained. The transition temperature from Regime II to Regime III was found to be about 120°C for both neat PLLA and PLLA/CHAp. The CHAp nanoparticles acted as an efficient nucleating agent, thus increasing the nucleation rate and decreasing the fold surface energy of PLLA. The nucleating agent effect of CHAp was also confirmed by the observations of smaller spherulites in PLLA using polarized optical microscopy.
4. The nonisothermal crystallization kinetics of neat PLLA and PLLA/CHAp nanocomposite were investigated with DSC at cooling rates range from 0.5 to 10°C/min. The combined Avrami-Ozawa equation was applied to analyze the nonisothermal crystallization process and the Ozawa exponent for neat PLLA and PLLA/CHAp were found to be very close to their Avrami exponent. According to the data obtained, the addition of CHAp only promoted the PLLA crystallization rate in the initial crystallization stage due to crystal germination

under the nonisothermal condition. Although in the isothermal condition, the addition of CHAp nanoparticles had influences on both crystal germination and growth mainly in Regime II.

5. Using the Kissinger equation, the nonisothermal crystallization activation energies of neat PLLA and PLLA/CHAp were found to be –149.67 and –124.91 kJ/mol, respectively. The differential isoconversion method by Friedman was applied to further estimate the dependence of the effective activation energy on the relative crystallinity and temperature for PLLA and PLLA/CHAp under nonisothermal crystallization. The LH parameters were obtained from the nonisothermal crystallization data as well by using the Vyazovkin-Sbirrazzuoli equation, and the values of U and K_g for neat PLLA and PLLA/CHAp were found to be 1846 J/mol and 7.52×10^5 K^2, 2565 J/mol and 6.37×10^5 K^2, respectively.

References

1. Wei, G.; Ma, P. X. Biomaterials 2004, 25, 4749.
2. Chen, Y.; Mak, A. F. T.; Wang, M.; Li, J.; Wong, M. S. Surf Coat Technol 2006, 201, 575.
3. Wang, M. Am J Biochem Biotechnol 2006, 2, 80.
4. Marega, C.; Marigo, A.; Dinoto, V.; Zannetti, R.; Martorana, A.; Paganetto, G. Makromol Chem 1992, 193, 1599.
5. Iannace, S.; Nicolais, L. J Appl Polym Sci 1997, 64, 911.
6. Miyata, T.; Masuko, T. Polymer 1998, 39, 5515.
7. Di Lorenzo, M. L. Eur Polym J 2005, 41, 569.
8. Piorkowska, E.; Galeski, A.; Haudin, J. M. Prog Polym Sci 2006, 31, 549.
9. Zhou, W. Y.; Lee, S. H.; Wang, M.; Cheung, W. L. Key Eng Mater 2007, 334, 1225.
10. Zhou, W. Y.; Lee, S. H.; Wang, M.; Cheung, W. L.; Ip, W. Y. J Mater Sci Mater Med 2008, 19, 2535.
11. German, R. M. In Sintering Theory and Practice; German, R. M., Ed.; Wiley: New York, 1996; Chapter 1, p 8.
12. Ignjatovic, N.; Suljovrujic, E.; Budinski-Simendic, J.; Krakovsky, I.; Uskokovic, D. J Biomed Mater Res 2004, 71, 284.
13. Zhou, W. Y.; Wang, M.; Cheung, W. L.; Guo, B. C.; Jia, D. M. J Mater Sci Mater Med 2008, 19, 103.
14. Zhou, W. Y.; Wang, M.; Cheung, W. L. Key Eng Mater 2007, 334, 1221.
15. Lever, T. In Thermal Analysis of Pharmaceuticals; Craig, D. Q. M., Reading, M., Eds.; CRC Press: Boca Raton, 2007; Chapter 2, p 30.
16. Arnoult, M.; Dargent, E.; Mano, J. F. Polymer 2007, 48, 1012.
17. Sosnowski, S. Polymer 2001, 42, 637.
18. Wu, D.; Wu, L.; Wu, L.; Xu, B. I. N.; Zhang, Y.; Zhang, M. J Polym Sci Part BPolym Phys 2007, 45, 1100.
19. Murariu, M.; Da Silva Ferreira, A.; Degee, P.; Alexandre, M.; Dubois, P. Polymer 2007, 48, 2613.
20. Lorenzo, A. T.; Arnal, M. L.; Albuerne, J.; Muller, A. J. Polym Test 2007, 26, 222.
21. Oca, H. M.d; Ward, I. M. J Polym Sci Part B Polym Phys 2007, 45, 892.
22. Tsuji, H.; Takai, H.; Saha, S. K. Polymer 2006, 47, 5430.
23. Kolstad, J. J. J Appl Polym Sci 1996, 62, 1079.
24. Pethrick, R. A. In Polymer Structure Characterization: From Nano to Macro Organization; RSC Publishing: Cambridge, UK, 2007; Chapter 6, p 158.
25. Krikorian, V.; Pochan, D. J. Macromolecules 2004, 37, 6480.
26. Hoffman, J. D.; Davis, G. T.; Lauritzen, J. I., Jr. In Treatise on Solid State Chemistry; Hannay, N. B., Ed.; Plenum Press, New York, 1976, Vol. 3, p 497.
27. Patki, R.; Mezghani, K.; Phillips, P. J. In Physical Properties of Polymers Handbook; Mark, J. E., Ed.; Springer: New York, 2007; Chapter 39, p 626.
28. Tjong, S. C.; Bao, S. P. J Polym Sci Part B Polym Phys 2005, 43, 253.
29. Hoffman, J. D.; Miller, R. L. Polymer 1997, 38, 3151.
30. Tsuji, H.; Miyase, T.; Tezuka, Y.; Saha, S. K. Biomacromolecules 2005, 6, 244.
31. Abe, H.; Kikkawa, Y.; Inoue, Y.; Doi, Y. Biomacromolecules 2001, 2, 1007.
32. Qiu, Z. B.; Yang, W. T. Polymer 2006, 47, 6429.
33. Di Lorenzo, M. L. Polymer 2001, 42, 9441.
34. Wittmann, J. C.; Lotz, B. Prog Polym Sci 1990, 15, 909.
35. Runt, J.; Miley, D. M.; Zhang, X.; Gallagher, K. P.; Mcfeaters, K.; Fishburn, J. Macromolecules 1992, 25, 1929.
36. Liao, R. G.; Yang, B.; Yu, W.; Zhou, C. X. J Appl Polym Sci 2007, 104, 310.
37. Chen, J. H.; Yao, B. X.; Su, W. B.; Yang, Y. B. Polymer 2007, 48, 1756.
38. Chen, C.; Fei, B.; Peng, S. W.; Zhuang, Y. G.; Dong, L. S.; Feng, Z. L. Eur Polym J 2002, 38, 1663.
39. Ozawa, T. Polymer 1971, 12, 150.
40. Di Lorenzo, M. L.; Silvestre, C. Prog Polym Sci 1999, 24, 917.
41. Kim, S. H.; Ahn, S. H.; Hirai, T. Polymer 2003, 44, 5625.
42. Lee, S. W.; Cakmak, M. J of Macromol Science, Part B 1998, 37, 501.
43. Jain, S.; Goossens, H.; Van Duin, M.; Lemstra, P. Polymer 2005, 46, 8805.
44. Liu, T.; Mo, Z.; Wang, S.; Zhang, H. Polym Eng Sci 1997, 37, 568.
45. Buzarovska, A.; Bogoeva-Gaceva, G.; Grozdanov, A.; Avella, M.; Gentile, G.; Errico, M. J Mater Sci 2007, 42, 6501.
46. Huang, H.; Gu, L.; Ozaki, Y. Polymer 2006, 47, 3935.
47. Kissinger, H. E. J Res Natl Inst Stand Technol 1956, 57, 217.
48. Ma, Y.; Hu, G.; Ren, X.; Wang, B. Mater Sci Eng A 2007, 460, 611.
49. Hao, Q.; Li, F.; Li, Q.; Li, Y.; Jia, L.; Yang, J.; Fang, Q.; Cao, A. Biomacromolecules 2005, 6, 2236.
50. Augis, J. A.; Bennett, J. E. J Therm Anal Calorimetry 1978, 13, 283.
51. Takhor, R. L. Advances in Nucleation and Crystallization of Glasses; American Ceramics Society: Columbus, 1971; p 166.
52. Vyazovkin, S. Macromol Rapid Commun 2002, 23, 771.
53. Friedman, H. L. J Polym Sci Part C 1964, 6, 183.
54. Vyazovkin, S.; Sbirrazzuoli, N. Macromol Rapid Commun 2006, 27, 1515.
55. Papageorgiou, G. Z.; Achilias, D. S.; Bikiaris, D. N. Macromol Chem Phys 2007, 208, 1250.
56. Vyazovkin, S.; Sbirrazzuoli, N. Macromol Rapid Commun 2004, 25, 733.
57. Achilias, D. S.; Papageorgiou, G. Z.; Karayannidis, G. P. Macromol Chem Phys 2005, 206, 1511.
58. Guo, B.; Zou, Q.; Lei, Y.; Du, M.; Liu, M.; Jia, D. Thermochim Acta 2009, 484, 48.